MINERALOGICAL MAGAZINE, SEPTEMBER 1974, VOL. 39, PP. 768–87

Some high-pressure pyroxenes

R. N. THOMPSON

Dept. of Geology, Imperial College of Science and Technology, London, SW7 2AZ

SUMMARY. Microprobe analyses of Ca-rich pyroxenes crystallized in the melting ranges of a magnesian alkali basalt, a transitional basalt, an olivine tholeiite, a tholeiitic andesite, and an augite leucitite at pressures between 8 and 45 kb show complex variation. Ca-poor pyroxene precipitated only from the alkali basalt at pressures between 14 and 18 kb. Pyroxene falling near the Di–Hed join in the pyroxene quadilateral formed at all pressures and temperatures from the leucitite, whereas 'Ca-rich' pyroxene crystallizing from the other four compositions was Ca-poor augite to sub-calcic augite. The *liquidus* Ca-rich pyroxenes all show rising Al and Na and falling Ti with increasing pressure and temperature. Other elements show complex behaviour; all but the leucitite pyroxenes tend to make temporary excursions of solid solution towards Ca-poor pyroxene at intermediate pressures, returning to more Ca-rich compositions at high pressures. At *sub-liquidus* temperatures Na and Ti consistently rise with falling T at constant P and also with rising P at constant T in these pyroxenes. The behaviour of the other elements in these circumstances depends on the nature of the coexisting phases.

Fe/Mg distribution between Ca-rich pyroxene and liquid, in the form

$$K_D = X^{Px}_{FeO} \cdot X^{Liq}_{MgO} / X^{Liq}_{FeO} \cdot X^{Px}_{MgO}.$$

has a constant value of 0·29 for three separate bulk compositions at widely differing temperatures and pressures. Distribution coefficients for Mg and Fe between pyroxenes and coexisting garnets at high pressures are very similar to those found in garnet pyroxenite xenoliths from Oahu, Hawaii. Systematic shifts in the apparent stoichiometry (all Fe taken as Fe^{2+}) of the augite leucitite pyroxenes are thought to indicate that they have considerable Fe^{3+} contents at low pressure, decreasing as P rises. If so, they show a strong negative correlation between Na and Fe^{3+}, which negates the customary practice of forming acmite before jadeite component when recalculating the analyses of high-pressure pyroxenes.

The sets of pyroxenes crystallized from each composition show consistent trends when plotted on such diagrams as jadeite *vs* Ca-Tschermak's 'molecule', which have often been used in attempts to discriminate natural pyroxenes formed in differing P–T environments. However, these new data show clearly that the bulk chemistry of the magma has a predominating influence on the composition of the pyroxenes crystallizing from it. Unless it is certain that a suite of natural pyroxenes have all precipitated from the same magma, it is probably pointless to attempt to deduce the relative P–T conditions of their formation from their major element chemistry.

IN recent years considerable attention has been paid to the possible use of the chemical compositions of pyroxenes as indicators of the physical conditions within the rocks containing them at the time of their formation. Many studies in this field have attempted to use the major element chemistry of pyroxenes found as megacrysts or polycrystalline inclusions within volcanic lavas and pyroclastic formations to delineate phases of high-pressure evolution in such rocks. In such attempts the chemical features of the naturally occurring minerals are compared with those of synthetic pyroxenes, formed under known P/T conditions. At present almost all the published data on pyroxenes crystallized experimentally at high pressures relates to simplified compositions, such as those in the system CaO–MgO–Al_2O_3–SiO_2 (Boyd, 1970), which lack

several of the elements forming substantial components of natural pyroxenes. Although the chemical variation of such pyroxenes as a function of P and T can be analysed rigorously within the context of the synthetic system from which they were formed, it is often difficult to extrapolate such results to the more complex chemistry and compositional trends shown by suites of naturally occurring pyroxenes and vice versa.

In an attempt to bridge this gap between experiment and nature, Ringwood, D. H. Green, and co-workers have published numerous electron-microprobe analyses of pyroxenes crystallized experimentally at high pressure from 'natural' basic and ultrabasic compositions (e.g. D. H. Green and Ringwood, 1967; T. H. Green and Ringwood, 1968; Bultitude and Green, 1971). Although contributing considerably to our understanding of high-pressure pyroxenes, these studies suffered from several deficiences. Firstly, the starting materials used in the experiments were not powders of naturally occurring rocks but, in most cases, synthetic glasses of hypothetical compositions 'modelled' (Bultitude and Green, 1971, p. 122) on known rock chemistries. Secondly, many of the pyroxene analyses were incomplete, with major element values 'calculated' or even 'assumed' (Green and Hibberson, 1970, table 4). Thirdly, the manual microprobe methods used when making the analyses necessitate relocating the electron beam on the chosen grain several times. This is exceedingly difficult to do when analysing the tiny crystals produced in an experimental run.

The data presented in this paper were obtained during an experimental study of the anhydrous melting behaviour of five lavas at pressures up to 45 kb. Preliminary P–T diagrams for two of the samples and details of the experimental techniques have already been published (Thompson, 1972). Major-element chemical analyses of both the crystalline and glassy products of many of the runs were made using the computer-automated MAC model 400 electron microprobe of the Geophysical Laboratory, Carnegie Institution of Washington (Finger and Hadidiacos, 1971). The pyroxenes crystallized in the experiments, which varied in size from 100 μm down to as little as 10 μm, could be analysed with this instrument without moving the electron beam from the chosen spot. The data thus obtained are discussed here with the objective of assisting our understanding of the factors controlling pyroxene chemistry.

Pyroxene analyses

The lavas used in the melting experiments were an alkali basalt and a transitional basalt from Skye, north-west Scotland, an olivine tholeiite and an iron-rich tholeiitic andesite from the Snake River Plain, Idaho, U.S.A., and an augite leucitite from Lago di Albano, Italy. Chemical analyses and CIPW norms of these rocks are given in Table I. Their melting behaviour at one atmosphere has previously been discussed by Tilley and Thompson (1970, 1972) and Thompson, Esson, and Dunham (1972). In the high-pressure experiments a Ca-rich pyroxene (augite or sub-calcite augite) was a prominent phase in the melting intervals of all five rocks studied. It was only accompanied by Ca-poor pyroxene within a narrow pressure range in one sample, the Skye alkali basalt. In the other composions it crystallized alone or with olivine, plagioclase, or garnet, in various combinations.

Complete studies of the varying chemistry of the pyroxenes precipitated throughout

the melting intervals of these lavas at various pressures would require very many more analytical data than have been collected so far in this study. In the more limited project reported here most of the analyses have been made of near-liquidus pyroxenes, but sufficient data are also available to show in a general way the effects of varying temperature at a given pressure.

Analytical techniques. The operating conditions of the microprobe were: accelerating potential 15 kv, specimen current 0·12 μa, and integration time on the scalers

TABLE I. *Chemical analyses of lavas used in the experiments*

	1	2	3	4	5		1	2	3	4	5
SiO_2	46·12	46·94	47·76	47·17	46·85	or	3·34	2·54	4·45	11·68	13·62
Al_2O_3	13·94	17·15	14·93	13·34	15·30	ab	20·96	25·12	22·01	28·82	—
Fe_2O_3	1·95	2·11	1·36	2·54	4·40	an	22·38	31·01	26·69	15·01	0·83
FeO	10·46	9·83	12·37	12·93	3·52	ne	2·84	0·19	—	—	13·63
MnO	0·18	0·19	0·20	0·23	0·17	lc	—	—	—	—	32·48
MgO	11·08	7·69	6·70	4·42	3·42	di	17·89	12·09	13·57	11·63	18·36
CaO	9·05	9·73	9·41	7·68	9·23	wo	—	—	—	—	7·42
Na_2O	3·11	3·01	2·62	3·40	2·97	hy	—	—	15·49	8·02	—
K_2O	0·57	0·43	0·75	2·00	9·26	ol	24·33	21·34	8·37	9·15	—
H_2O^+	1·49	1·55	nil	0·33	0·81	il	3·50	2·60	5·78	7·90	6·08
H_2O^-	0·40	nil	0·03	0·15	nil	mt	2·90	2·18*	2·09	3·71	2·55
TiO_2	1·81	1·37	3·03	4·15	3·25	hm	—	—	—	—	2·73
P_2O_5	0·23	0·18	0·53	1·39	0·65	ap	0·34	0·39	1·16	3·36	1·42
CO_2	—	0·06	0·01	0·04	nil	ct	—	0·14	0·04	0·10	—
Total	100·39	100·24	99·70	99·77	99·83						
Mg/(Mg+Fe)	0·62	0·54	0·47	0·34	0·45						
Ca/(Ca+Mg+Fe)	0·27	0·33	0·32	0·30	0·47						

* Fe_2O_3 set at 1·50 % for calculation of this norm, to conform with the procedure of Thompson *et al.* (1972).

1. Olivine-rich alkali basalt (66018), Achtalean, Skye, north-west Scotland; analyst: J. H. Scoon (Tilley and Muir, 1962)
2. Transitional basalt (SK 971), Fairy Bridge, Skye, north-west Scotland; analyst: J. Esson (Thompson *et al.*, 1972).
3. Olivine tholeiite (59-P-13), McKinney basalt, Snake River Plain, Idaho, U.S.A.; analyst: D. F. Powers (Tilley and Thompson, 1970).
4. Tholeiitic andesite (OB 32), King Hill, Snake River Plain, Idaho, U.S.A.; analyst: P. Montalto (Tilley and Thompson 1970).
5. Augite leucitite (EU 13), Lago di Albano caldera, nr. Rome, Italy; analyst: Geochemical Laboratories, Manchester University (Tilley and Thompson, 1972).

The numbers given to these specimens are those used in previously published studies of them.

30 seconds. The standards used were glass of the composition 65 % $CaMgSi_2O_6$ 35 % $NaAlSi_2O_6$ for Si, Al, Ca, Mg, and Na; Ti, Cr, and Mn-doped glasses of garnet and pyroxene compositions for Fe, Ti, Cr, and Mn; orthoclase for K (Boyd, 1968). Raw data were corrected by the method of Bence and Albee (1968) and are thought to be accurate to ± 2 % for elements exceeding 10 % in an analysis and ± 5 % or more for elements present in lesser amounts.

One of the most difficult problems encountered when analysing with the microprobe the miniscule crystals formed during anhydrous runs is to ensure that the volume excited by the incident electron beam is confined to one crystal, so that the analysis is not contaminated by surrounding material either on or *below* the polished surface. The near-liquidus pyroxenes used in the present study were always surrounded by glass. Potassium only enters the pyroxene lattice in trace quantities at high pressures (Erlank and Kushiro, 1970). Therefore, the K_2O recorded in each analysis was taken as a monitor of the amount of glass inadvertently included in that spot. The

minimum K_2O value attained varied according to the K_2O content of the rock. Presumably this was due to excitation of potassium in glass outside the main analysed volume by secondary X-ray fluorescence or possibly to minute inclusions of glass within the pyroxene crystals. Five individual analyses with minimal K_2O contents were averaged for each run wherever possible.

Quality of analyses. The analyses of the near-liquidus high-pressure pyroxenes in the five lavas are given in Table II. The average total of all the analyses used in this study is 100·1. If all the iron is calculated as FeO, the average cation sum on a 6 oxygen basis is 4·00. The experiments were made with powdered rock contained within graphite capsules. These buffer the charges at values of f_{O_2} within the field of stability of wüstite in the system Fe–C–O, at the pressures and temperatures used in this study (Thompson and Kushiro, 1972). It would therefore seem reasonable to assume that the pyroxenes are essentially free from Fe^{3+} (but see below concerning the EU 13 leucitite pyroxenes).

Chemical variation in near-liquidus pyroxenes. As very few of the pyroxenes crystallized in this study were the Ca-poor species, the term pyroxene will be used without qualification in this section to refer to Ca-rich pyroxene augite or sub-calcic augite. The chemical variation observed in sets of near-liquidus pyroxenes (Table II) results from the interplay of the competing influences of bulk rock composition, co-existing phases, pressure, and temperature on the mineral. The liquidus curves of all five studied specimens are positive on a *P–T* diagram (except for a negative section at relatively low pressures in the part of the leucitite liquidus curve where leucite is the primary phase). Therefore, the sets of near-liquidus pyroxenes in Table II show the effects of both rising pressure *and* temperature. Another point to remember is that the analyses are not of course all of true liquidus pyroxenes, the first few crystals to form on cooling at a given pressure. Their deviation from this ideal is noted on Table II and should be borne in mind when considering the variation of elements particularly sensitive to temperature.

Inspection of Table II shows the importance of the bulk composition of the system in controlling the composition (and species) of the near-liquidus pyroxene precipitating from it. Most of the pyroxenes in Table II crystallized in the *P–T* range of 8 to 35 kb and 1200 to 1450 °C. Nevertheless, the groups of pyroxenes in Table II that precipitated from the various lavas are quite distinct chemically, although the differences between some of the latter are not large (Table I). Several aspects of the chemical variation recorded in Table II are shown diagrammatically in figs. 1 to 3. Specific cases of the influence of bulk composition on pyroxene chemistry will be noted during the description of these diagrams.

The behaviour of the elements considered in Table II, as functions of pressure and temperature along the 'liquidus pyroxene trends', is of several types. Cr and Mn apparently show no consistent variation within pyroxene sets, although their abundances vary appreciably from group to group. Al correlates positively with pressure in all the pyroxene sets (fig. 1). On the other hand, it is clear that the chemical factors controlling the over-all levels of Al in each set are complex. With one exception, the most aluminous pyroxene crystallized at a given pressure in this study was always

TABLE II. *Microprobe analyses of high pressure pyroxenes*

Bulk comp.	66018 Olivine-rich alkali basalt									SK 971 Transitional basalt						59-P-13 Olivine tholeiite			
Pres. (kb)	10	14	15	17	17	20	24	28	31	13	15	18	20	23	26	8	9	10	12
Temp. (°C)	1225	1300	1325	1360	1360	1310	1400	1440	1475	1275	1275	1325	1350	1375	1380	1175	1200	1200	1225
°C below est. liq.	105	50	35	15	15	45	50	50	50	20	25	25	30	50	90	30	10	20	20
Pyroxene type*	Cpx	Cpx	Opx	Cpx	Pig	Cpx	Cpx	Cpx	Cpx	Cpx	Cpx	Cpx	Cpx	Cpx	Cpx	Cpx	Cpx	Cpx	Cpx
Other solids	Ol	Ol	Cpx	Pig	Cpx	—	—	Gt	Gt	—	—	—	—	—	Gt	Pl, Ol	Pl	Pl	Pl
SiO_2	50·7	51·2	53·6	52·2	55·0	52·1	50·3	50·3	50·3	49·7	49·1	49·9	49·4	49·2	47·6	50·2	50·4	50·3	50·2
Al_2O_3	5·64	6·13	4·77	6·39	3·55	6·84	9·54	9·78	10·8	9·54	9·73	10·5	10·8	13·2	15·6	4·27	4·49	5·21	7·05
FeO†	8·73	9·70	10·1	9·29	9·40	9·14	8·79	9·25	8·21	9·25	10·1	8·31	8·22	8·62	8·64	14·2	12·8	12·9	11·8
MnO	0·20	0·20	0·20	0·20	0·20	0·21	0·21	0·19	0·20	0·20	0·18	0·16	0·17	0·15	0·16	0·33	0·30	0·34	0·27
MgO	18·6	21·8	29·2	24·3	29·0	22·0	18·0	17·1	17·4	16·4	15·6	15·7	14·9	13·8	11·5	17·0	18·5	18·6	16·8
CaO	13·6	8·90	1·82	6·01	2·84	8·04	10·6	10·7	10·6	13·5	12·9	14·1	14·5	13·6	13·8	12·0	11·0	10·7	12·5
Na_2O	0·56	0·59	0·10	0·51	0·23	0·85	1·43	1·57	1·88	0·71	0·86	1·13	1·25	1·46	2·14	0·36	0·40	0·36	0·57
K_2O	0·02	0·02	0·00	0·01	0·00	0·02	0·03	0·03	0·01	0·00	0·00	0·00	0·00	0·02	0·00	0·01	0·03	0·01	0·01
TiO_2	0·85	0·49	0·33	0·50	0·24	0·44	0·47	0·96	0·55	0·69	0·72	0·50	0·62	0·67	0·63	1·51	1·44	1·16	1·40
Cr_2O_3	1·05	0·45	0·37	0·53	0·37	0·41	0·32	0·23	0·33	0·12	0·09	0·12	0·09	0·08	0·05	0·14	0·23	0·14	0·20
Total	100·0	99·5	100·5	99·9	100·8	100·1	99·7	100·1	100·3	100·1	99·3	100·4	100·0	101·8	100·1	100·0	99·6	99·7	100·8
Cations on the basis of 6 oxygens																			
Si	1·854	1·858	1·884	1·865	1·924	1·868	1·821	1·821	1·808	1·808	1·807	1·806	1·798	1·771	1·730	1·869	1·866	1·860	1·832
Al^{iv}	0·146	0·142	0·116	0·135	0·076	0·132	0·179	0·179	0·192	0·192	0·193	0·194	0·202	0·229	0·270	0·131	0·134	0·140	0·168
Al^{vi}	0·096	0·120	0·081	0·133	0·070	0·156	0·228	0·237	0·265	0·217	0·229	0·254	0·260	0·329	0·398	0·056	0·061	0·087	0·135
Cr	0·030	0·013	0·009	0·015	0·010	0·011	0·008	0·006	0·008	0·003	0·002	0·003	0·002	0·002	0·001	0·003	0·006	0·003	0·005
Fe	0·266	0·294	0·296	0·276	0·275	0·273	0·266	0·279	0·247	0·281	0·309	0·250	0·250	0·259	0·262	0·442	0·396	0·397	0·360
Mn	0·005	0·005	0·005	0·005	0·005	0·005	0·006	0·005	0·005	0·005	0·005	0·004	0·004	0·004	0·004	0·010	0·008	0·010	0·007
Mg	1·012	1·180	1·533	1·292	1·512	1·175	0·973	0·919	0·931	0·890	0·856	0·844	0·810	0·742	0·623	0·942	1·022	1·027	0·917
Ti	0·022	0·013	0·008	0·012	0·006	0·011	0·013	0·025	0·015	0·018	0·019	0·013	0·016	0·018	0·017	0·042	0·039	0·031	0·037
Ca	0·534	0·346	0·068	0·229	0·105	0·308	0·412	0·414	0·407	0·527	0·508	0·547	0·565	0·522	0·535	0·479	0·436	0·423	0·486
Na	0·040	0·040	0·010	0·034	0·015	0·059	0·100	0·110	0·130	0·050	0·060	0·078	0·087	0·101	0·150	0·026	0·028	0·026	0·040
K	0·001	0·000	0·000	0·000	0·000	0·000	0·001	0·001	0·000	0·000	0·000	0·000	0·000	0·001	0·000	0·000	0·001	0·000	0·000
Σ	4·006	4·010	4·006	3·997	3·998	3·998	4·007	3·997	4·008	3·990	3·988	3·993	3·993	3·978	3·990	3·998	3·998	4·003	3·987
Mg/(Mg+Fe)	0·79	0·80	0·84	0·82	0·85	0·81	0·79	0·77	0·79	0·76	0·74	0·77	0·76	0·74	0·70	0·68	0·72	0·72	0·72
Pyroxene components (Mol. per cent)																			
$CaTiAl_2O_6$	2·2	1·3		1·2		1·1	1·3	2·5	1·4	1·8	1·9	1·3	1·6	1·8	1·7	4·2	3·9	3·1	3·7
$NaAlSi_2O_6$	4·1	4·0		3·4		5·9	10·0	11·1	12·9	5·0	6·1	7·8	8·7	10·4	15·1	2·6	2·9	2·6	4·0
$CaAl_2SiO_6$	9·3	10·4		11·3		10·9	14·3	13·1	15·1	16·4	16·5	17·5	17·4	21·4	24·5	4·0	4·7	7·1	9·8
$Ca_2Si_2O_6$	20·7	11·3		5·2		9·4	12·7	12·9	11·9	17·4	16·5	18·1	18·9	15·0	13·9	19·8	17·4	16·0	17·7
$Mg_2Si_2O_6$	50·2	58·3		64·7		58·8	48·3	46·1	46·1	44·9	43·2	42·5	40·7	37·9	31·4	46·9	51·0	51·0	46·2
$Fe_2Si_2O_6$	13·5	14·8		14·1		13·9	13·5	14·2	12·5	14·4	15·8	12·8	12·8	13·5	13·4	22·5	20·1	20·2	18·5

* Abbreviations are: Cpx = Ca-rich clinopyroxene (including sub-calcic augite); Pig = Pigeonite; Opx = Orthopyroxene; Ol = Olivine; Pl = Plagioclase; Lc = Leucite; Gt = Garnet; Sp = Fe-Ti spinel.

† All Fe assumed to be FeO (see text for discussion).

Bulk comp.	59-P-13 Olivine tholeiite				OB 32 Tholeiitic andesite						EU 13 Augite leucitite							
Pres. (kb)	15	18	25	34	8·5	15	17	24	26	29	10	15	16	20	24	28	33	32
Temp. (°C)	1250	1300	1375	1450	1125	1200	1225	1300	1325	1350	1200	1250	1275	1300	1335	1350	1350	1475
°C below est. liq.	25	10	5	25	20	20	15	10	5	10	70	20	5	15	15	30	75	25
Pyroxene type*	Cpx	Cpx	Cpx	Cpx	Cpx	Cpx	Cpx	Cpx	Cpx	Cpx	Cpx	Cpx	Cpx	Cpx	Cpx	Cpx	Cpx	Cpx
Other solids	—	—	—	Gt	Pl, Ol Sp	—	—	—	Gt	Gt	Lc	—	—	—	—	—	—	—
SiO_2	49·8	50·0	50·7	51·3	49·0	48·6	49·8	49·3	49·3	49·2	45·5	45·6	46·1	46·1	45·6	45·7	45·4	45·7
Al_2O_3	7·64	10·3	10·1	12·0	3·66	6·91	7·08	9·82	10·1	11·1	9·22	10·9	10·9	12·0	13·7	15·1	16·0	18·1
FeO†	11·4	11·5	9·15	8·75	18·3	14·2	12·6	13·6	12·5	11·8	8·94	8·07	7·46	7·44	7·00	6·63	6·96	5·26
MnO	0·28	0·21	0·22	0·22	0·44	0·33	0·29	0·30	0·29	0·23	0·14	0·15	0·16	0·13	0·13	0·18	0·16	0·12
MgO	16·5	13·4	15·4	13·0	14·9	12·3	12·8	10·2	10·5	9·89	10·9	10·7	10·7	10·1	9·55	8·93	8·02	8·28
CaO	12·3	12·5	12·6	13·4	10·7	13·4	14·5	13·4	12·8	13·4	23·2	22·5	22·7	21·7	21·7	20·6	20·3	20·0
Na_2O	0·71	1·18	1·46	2·29	0·45	1·05	1·21	2·28	2·29	2·63	0·44	0·56	0·78	0·92	1·09	1·51	1·75	2·27
K_2O	0·01	0·14	0·00	0·00	0·05	0·03	0·03	0·03	0·10	0·04	0·10	0·12	0·16	0·14	0·12	0·14	0·23	0·14
TiO_2	1·31	1·54	0·81	0·82	1·36	1·71	1·42	1·37	1·48	1·30	1·26	0·98	0·67	0·65	0·74	0·69	0·53	0·39
Cr_2O_3	0·20	0·09	0·24	0·08	0·01	0·01	0·00	0·00	0·00	0·00	0·00	0·00	0·00	0·00	0·00	0·00	0·00	0·00
Total	100·2	100·9	100·7	101·9	98·9	98·5	99·7	100·3	99·4	99·6	99·7	99·6	99·6	99·2	99·6	99·5	99·4	100·3
Cations on the basis of 6 oxygens																		
Si	1·827	1·816	1·827	1·826	1·878	1·847	1·856	1·831	1·837	1·827	1·721	1·713	1·726	1·726	1·698	1·694	1·687	1·666
Al^{iv}	0·173	0·184	0·173	0·174	0·122	0·153	0·144	0·169	0·163	0·173	0·279	0·287	0·274	0·274	0·302	0·306	0·313	0·334
Al^{vi}	0·156	0·257	0·256	0·328	0·043	0·156	0·167	0·260	0·280	0·309	0·132	0·194	0·209	0·257	0·299	0·355	0·389	0·442
Cr	0·005	0·002	0·006	0·002	0·000	0·000	0·000	0·000	0·000	0·000	0·000	0·000	0·000	0·000	0·000	0·000	0·000	0·000
Fe	0·351	0·348	0·275	0·260	0·587	0·452	0·394	0·421	0·388	0·366	0·282	0·253	0·233	0·233	0·217	0·206	0·216	0·159
Mn	0·008	0·005	0·006	0·006	0·013	0·010	0·008	0·008	0·008	0·006	0·004	0·004	0·004	0·003	0·003	0·005	0·004	0·003
Mg	0·899	0·723	0·825	0·691	0·852	0·697	0·711	0·565	0·581	0·546	0·616	0·600	0·598	0·565	0·530	0·493	0·444	0·449
Ti	0·035	0·042	0·021	0·021	0·038	0·048	0·039	0·038	0·040	0·036	0·035	0·027	0·019	0·018	0·021	0·018	0·014	0·010
Ca	0·481	0·486	0·488	0·508	0·438	0·543	0·578	0·531	0·508	0·531	0·941	0·907	0·912	0·871	0·864	0·818	0·808	0·781
Na	0·049	0·082	0·102	0·158	0·032	0·077	0·087	0·163	0·165	0·188	0·031	0·040	0·056	0·066	0·077	0·107	0·125	0·159
K	0·000	0·006	0·000	0·000	0·002	0·001	0·001	0·001	0·004	0·001	0·004	0·005	0·007	0·006	0·005	0·005	0·010	0·005
Σ	3·985	3·950	3·979	3·973	4·006	3·983	3·986	3·989	3·974	3·983	4·046	4·031	4·037	4·019	4·016	4·008	4·009	4·008
Mg/(Mg+Fe)	0·72	0·68	0·75	0·73	0·59	0·61	0·64	0·57	0·60	0·60	0·69	0·70	0·72	0·71	0·71	0·71	0·67	0·74
Pyroxene components (Mol. per cent)																		
$CaTiAl_2O_6$	3·6	4·4	2·1	2·1	3·8	4·9	3·9	3·8	4·1	3·7	3·3	2·6	1·8	1·8	2·1	1·8	1·4	1·0
$NaAlSi_2O_6$	5·0	9·2	10·4	16·2	3·3	7·9	8·9	16·5	17·2	19·1	3·3	4·3	6·1	7·0	9·0	11·0	13·3	16·2
$CaAl_2SiO_6$	10·0	14·2	14·8	15·5	2·8	6·9	7·4	9·6	9·9	11·2	14·6	18·4	18·3	20·7	23·3	26·3	26·6	29·2
$Ca_2Si_2O_6$	17·6	16·1	16·4	17·2	18·4	21·7	23·5	20·0	19·0	19·5	35·9	33·3	33·7	31·3	30·0	26·3	25·9	23·5
$Mg_2Si_2O_6$	45·6	37·7	42·0	35·4	42·1	35·3	36·0	28·5	29·7	27·7	29·3	28·9	28·7	27·6	25·9	24·3	21·9	22·2
$Fe_2Si_2O_6$	18·2	18·5	14·3	13·6	29·7	23·4	20·3	21·6	20·2	18·8	13·6	12·4	11·4	11·5	10·7	10·4	10·9	8·0

from EU 13, the most strongly silica-undersaturated rock (fig. 1). However, the second most strongly silica-undersaturated rock, 66018, precipitated the least aluminous pyroxenes at all but one of the pressures plotted on fig. 1. The relatively high Al_2O_3 (Table I) in SK 971 could explain the relatively aluminous nature of the pyroxenes precipitated from it. The data for Ti are very scattered (fig. 2) and, if anything, seem to show a slight negative correlation with pressure. Neither the silica-saturation nor the TiO_2 contents of the rocks (Table I) correlate with the Ti levels in the pyroxene sets.

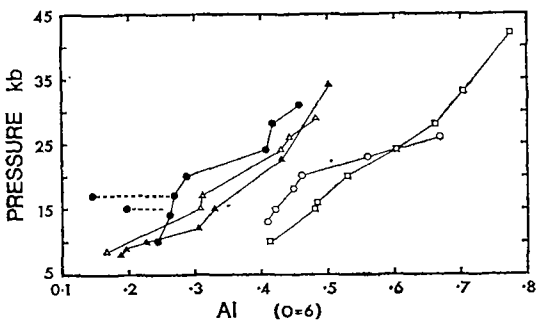

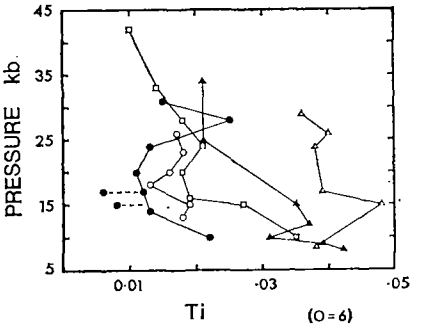

FIGS. 1 and 2: FIG. 1 (left). Al versus pressure for the near-liquidus pyroxenes of Table II. The symbols denote the sets of pyroxenes crystallizing from the five bulk compositions listed in Table I as follows: filled circles = olivine-rich alkali basalt 66018; open circles = transitional basalt SK971; filled triangles = olivine tholeiite 59-P-13; open triangles = tholeiitic andesite OB32; open squares = augite leucitite EU13. A broken line joins coexisting Ca-rich pyroxene and pigeonite in 66018 at 17 kb. FIG. 2 (right). Ti versus pressure for the near-liquidus pyroxenes of Table II. Symbols as in fig. 1.

If the pyroxenes in the EU 13 (augite leucitite) set in Table II are considered alone, the variation of the remaining elements seems quite straightforward. Si shows no consistent trend with rising pressure, whilst Na rises and Fe, Mg, and Ca all fall steadily. However, EU 13 is much more strongly silica-undersaturated and has a considerably higher Ca/(Ca+Mg+Fe) ratio than the other four lavas studied (Table I). The latter precipitate relatively silica-rich and sub-calcic 'Ca-rich pyroxenes', which show rather complex substitutions along the near-liquidus trends. These features are best seen in the 66018 (alkali basalt) set. With rising temperature and pressure the Ca-rich pyroxenes become progressively poorer in Ca (fig. 3) and Na and richer in Si, Mg, and Fe. Thus they show solid solution towards Ca-poor pyroxene and, indeed, co-precipitate with both hypersthene and pigeonite at pressures between 15 and 17 kb. At higher pressures the Ca-poor pyroxenes cease to precipitate near the liquidus and the Ca-rich phase becomes progressively richer in Ca and Na and poorer

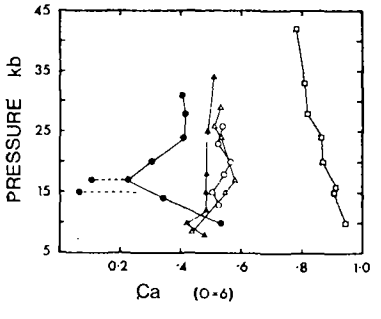

FIG. 3. Ca versus pressure for the near-liquidus pyroxenes in Table II. Symbols as in fig. 1.

in Si, Mg, and Fe. At the highest pressures, 28 to 31 kb, attained in the 66018 set the elements Si, Ca, Mg, and Fe cease to vary measurably whilst Na continues to rise.

All this complex variation in the 66018 pyroxenes may be incorporated into the following statements: The main chemical trend in all the pyroxenes in Table II is one of increasing Al and Na with rising pressure (and temperature), at the expense of the other major elements. However, in 66018 a temporary excursion of substitutions towards Ca-poor pyroxene is superimposed on the main trend at intermediate pressures. This does not greatly affect the progressive substitution of Al in the series but temporarily reduces that of Na, because this element is much less soluble in Ca-poor than in Ca-rich pyroxene at a given pressure and temperature (see the 17 kb 66018 pyroxenes in Table II).

The variation of Si, Ca, Mg, Fe, and Na in the 59-P-13, OB32, and SK 971 pyroxene sets (Table II) can be fitted to the pattern described for 66018. The 59-P-13 and SK 971 pyroxenes show small but distinct substitutional excursions towards Ca-poor pyroxene at intermediate pressures (fig. 3). The OB 32 pyroxenes show between 8·5 and 17 kb the same pattern of chemical variation as that in 66018 pyroxenes between 17 and 24 kb. As with elements previously discussed, there appears to be no simple parameter, such as silica-saturation or Ca/(Ca+Mg+Fe) ratio, that relates the levels of Si, Ca, Mg, Fe, and Na in the pyroxene sets to the chemistry of the compositions from which they precipitated. The only partial exception to this lack of simple pattern concerns Fe and Mg. If just the most magnesian Ca-rich pyroxene in each set in Table II is considered, the Mg/(Mg+Fe) ratios of these five analyses fall in the same order as the Mg/(Mg+Fe) ratios of the rocks from which they were precipitated. The Mg/(Mg+Fe) ratios of the remaining pyroxenes in each set correlate negatively with the distance below the estimated liquidus temperature (Table II) at which they crystallized.

Separation of the effects of pressure and temperature. The ambiguity as to the relative effects of pressure and temperature in determining the chemical trends discussed above can largely be resolved by considering the variation at constant pressure and varying temperature and vice versa in pyroxenes crystallized from each lava. Even this procedure is not without complications, because the influence of the various other phases crystallizing with the pyroxenes must also be taken into account. The analyses used in this section will be published when the melting behaviours of the five rocks are discussed and meanwhile may be obtained from the author.

All the analysed sets (pairs and trios) of pyroxenes show decreases in Mg, increases in Fe, and therefore decreases in their Mg/(Mg+Fe) ratios with falling temperature at constant pressure. Cr, like Mg, decreases sharply in these pyroxenes at constant P and falling T.

The available data for the remaining six elements studied are plotted in figs. 4 to 6. Na and Ti (fig. 4) both increase with falling temperature at a given pressure. There are more sets of analyses for 59-P-13 than for the other lavas. If the data for this rock are extrapolated a little on fig. 4, it is possible to estimate the effect of rising pressure at a constant temperature of 1225 °C for these pyroxenes. It appears that, at this temperature, both Na and Ti increase sharply with rising pressure. This effect of pressure is opposed by that of temperature in the near-liquidus pyroxene trends. The final

result of Na rising and Ti falling along the trends is a compromise between these influences.

The variation of Mn in fig. 5 resembles that of Na and Ti in fig. 4, except that the 26 and 34 kb 59-P-13 pyroxene pairs, which co-precipitated with abundant relatively Mn-rich garnet (unpublished analyses), show decreasing Mn contents with falling temperature. Despite several obvious exceptions, there seems to be a general tendency for both Ca (fig. 5) and Si (fig. 6) to decrease with falling T at constant P. The 17 kb 66018 sub-calcic augites coexist with Ca-poor pyroxenes and their trend of rising Ca with falling T reflects the operation of the pyroxene solvus. The complex variation of Al in fig. 6 contrasts with its behaviour in the near-liquidus pyroxene trends (fig. 1). The data mostly fit quite well to a pattern of increasing Al with decreasing temperature, except where the pyroxene coexists with abundant garnet (this is in the 59-P-13 pairs at 34 and 26 kb and in the 25 kb set at temperatures below 1350 °C). The Si variation (fig. 6) shows a complementary pattern. At 1175 °C and pressures below the stability field of garnet, the 59-P-13 pyroxenes show falling Si and Ca and rising Al (figs. 5 and 6) with rising pressure.

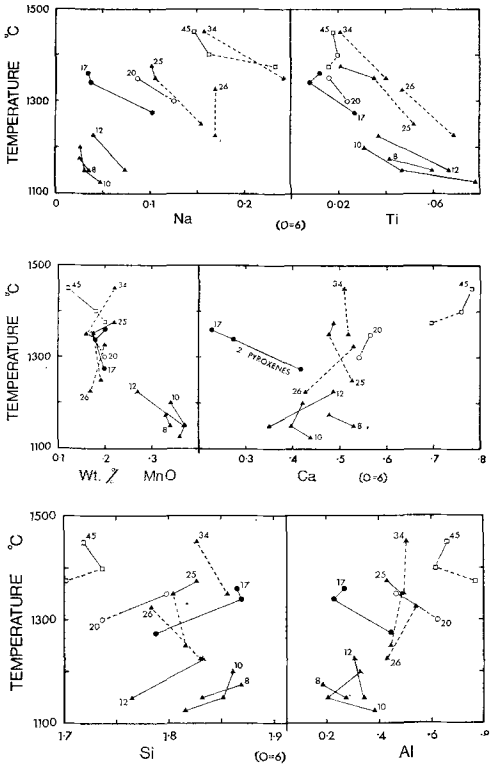

FIGS. 4, 5, 6: FIG. 4 (top). Na and Ti versus temperature for pyroxenes crystallized at various constant pressures from the bulk compositions of Table I. Symbols as in fig. 1. Broken lines denote temperature ranges where pyroxene coexists with garnet (plus liquid). Solid lines denote temperature ranges where pyroxene coexists with phases other than garnet. The pressure of crystallization (in kb) is marked beside each isobaric polythermal set. FIG. 5 (middle). MnO and Ca versus temperature for the pyroxenes shown in fig. 4. Symbols as in figs. 1 and 4. FIG. 6 (bottom). Si and Al versus temperature for the pyroxenes shown in fig. 4. Symbols as in figs. 1 and 4.

Discussion of new and earlier data

The very sub-calcic Ca-rich pyroxenes in the 66018, 59-P-13, and OB 32 sets (Table II) are reminiscent of the pyroxenes in a Picture Gorge basalt from Oregon, U.S.A., which were deduced by Smith and Lindsley (1971) to be metastable products of rapid quenching. However, the following points support the proposal that these are truly equilibrium compositions: Firstly, the starting materials were rock powders, so that all but the largely vitreous basalt 59-P-13 contained pyroxene fragments to act as nuclei. Secondly, run lengths varied from 0·5 to 6 hours but showed no correlation

between run length and amount or chemistry of pyroxene produced. Thirdly, the consistent nature of the chemical trends within the pyroxene sets in Table II is an unlikely, although not impossible, result of metastable crystallization. Finally, the strongly silica-undersaturated and relatively calcic composition, EU 13, precipitates a Ca-rich pyroxene falling close to the Di–Hed join in the pyroxene quadilateral at all pressures and temperatures investigated.

Ca, Mg, and Fe distributions amongst the pyroxenes. If these pyroxenes are accepted as equilibrium compositions, it is interesting to consider their Ca, Mg, and Fe contents in relation to previous studies of the distribution of these elements amongst crystalline

TABLE III. Fe/Mg *distribution between high-pressure pyroxenes and liquid*

Rock*	Pressure	Temperature	K_D†
59-P-13	25kb	1375 °C	0·29
OB 32	17	1225	0·29
EU 13	42	1475	0·29
SK 971	18	1325	0·35
66018	20	1310	0·38

* Rock composition (Table I) taken as liquid composition at liquidus.
† $K_D = X^{Px}_{FeO} \cdot X^{Liq}_{MgO} / X^{Liq}_{FeO} \cdot X^{Px}_{MgO}$.
All Fe taken as FeO.

and liquid phases in various synthetic and natural systems. Roeder and Emslie (1970) determined Fe^{2+}/Mg distribution experimentally in the equilibrium olivine+liquid at one atmosphere in basaltic compositions. They found that a distribution coefficient $K_D = X^{Ol}_{FeO} \cdot X^{Liq}_{MgO} / X^{Liq}_{FeO} \cdot X^{Ol}_{MgO}$ (where X^{Ol}_{FeO} is the mole fraction of FeO in olivine, *et sim.*) relating Fe^{2+} and Mg partitioning between olivine and liquid had a constant average value of 0·30 throughout the range of bulk compositions and physical conditions they studied. The equilibrium Ca-rich pyroxene+liquid cannot be studied in basaltic melts at one atmosphere, because it is very rare for Ca-rich pyroxene to precipitate unaccompanied by other phases (Thompson and Flower, 1971). However, many mafic lavas, including all those studied here, have fields of Ca-rich pyroxene+liquid at high pressures in their *P-T* diagrams. The charges produced in the high pressure runs are too small to analyse for Fe^{2+} and Fe^{3+} and all the iron in them must be assumed to be Fe^{2+}. As pointed out previously, this is a reasonable assumption, except perhaps for the augite leucitite. Unfortunately, no microprobe analyses have been made in the present study of the glasses coexisting with Ca-rich pyroxene alone. Therefore, distribution coefficients may only be calculated for liquidus runs, where the bulk composition can be taken as the liquid.

Table III shows the results of this calculation for the Ca-rich pyroxene with the highest Mg/Fe ratio from each set in Table II. If the chosen pyroxene crystallized appreciably below the liquidus, the distribution coefficient calculated by this method will be greater than the true value. Three of the pyroxene-liquid pairs in Table III have identical K_D values of 0·29. The constancy of this coefficient in three separate bulk compositions, equilibrated over a wide range of pressures and temperatures, is remarkable and akin to the relationship for olivine–liquid reported by Roeder and Emslie (1970). The two remaining K_D values in Table III exceed 0·29 and, as might be

expected, are from runs containing several percent of crystals. Therefore, although no suitable data are available to calculate true values of K_D for 66018 and SK 971, the results given in Table III are compatible with the figure of 0·29.

Banno and Matsui (1965) considered the distribution of Fe and Mg between pyroxenes and garnets in eclogites from various geological environments. They showed that the distribution coefficient $K' = \ln(X^{Gt}_{Mg}.X^{Cpx}_{Fe}/X^{Gt}_{Fe}.X^{Cpx}_{Mg})$ varied considerably and suggested that it correlated inversely with temperature of formation of the assemblage. The expanded version of Banno and Matsui's data given by Lovering and White (1969) is summarized in fig. 7. On this diagram are plotted Fe/Mg ratios for the coexisting Ca-rich pyroxenes and garnets analysed during the present study. The garnet analyses will be published when the melting behaviour of the rocks is described. The new data define a field on fig. 7 of pyroxene–garnet pairs in equilibrium with mafic liquids that falls at slightly lower values of K' than any of the naturally occurring assemblage groups plotted by Lovering and White (1969). Previous analyses by Green and Ringwood (1968) and Bultitude and Green (1971) fall in the same general field in fig. 7 as the new data and extend it towards lower Fe/Mg ratios. Green and Ringwood's analyses show slightly lower values of K' than the results reported here.

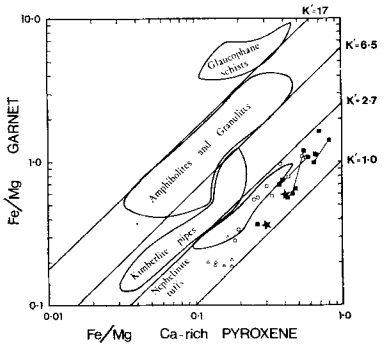

FIG. 7. Distribution of Fe and Mg between coexisting Ca-rich pyroxene and garnet from different geological environments and experimental melting studies. The values of K' separating the various environments are those suggested by Banno and Matsui (1965). The labelled fields are as compiled by Lovering and White (1969). Filled squares denote the newly analysed experimental pyroxene–garnet pairs. Tie lines join assemblages formed at different temperatures under constant pressure. The symbols for previously published experimental data are: open squares, Green and Ringwood (1968); open triangles, Bultitude and Green (1971). Stars are garnet pyroxenite xenoliths from Salt Lake Crater, Oahu (Beeson and Jackson, 1970).

Only two naturally occurring pyroxene–garnet pairs plot amongst the new experimental data points on fig. 7. Both of these are garnet pyroxenites from Salt Lake Crater, Oahu. One is 'as analysed' by Beeson and Jackson (1970); the other is a 'recalculated' assemblage, computed by these authors from chemical and modal data on a xenolith containing phases showing complex exsolution. The unrecalculated Salt Lake Crater analyses fall in the field of garnet pyroxenites from nephelinite tuffs (which is what they are) on fig. 7. Other points in this field, from the Delegate breccia pipes, N.S.W., Australia (Lovering and White, 1969), are also pyroxene–garnet assemblages that show exsolution features, suggesting partial solid-state re-equilibration to temperatures or pressures (or both) below those at which they formed. If the garnet pyroxenites in the nephelinite tuff field of fig. 7 originally formed in equilibrium with mafic liquids, their present K' values after partial re-equilibration at lower temperatures conform with the hypothesis of Banno and Matsui (1965). This point is confirmed by four pairs of pyroxene–garnet assemblages analysed in the present study (fig. 7), which show the

effects of falling temperature at constant pressure. In each case the lower temperature member of the pair has the higher K' value.

As only one coexisting Ca-rich and Ca-poor pyroxene pair was analysed in the present study, the new data give little information about the shape of the two-pyroxene solvus in complex pyroxene systems. However, the narrowness of the compositional gap between the two pyroxenes precipitated from 66018 at 17 kb and 1360 °C (Table II and fig. 3) contrasts with the width of the Fe-free pyroxene solvus at this temperature (Boyd and Schairer, 1964; Davis and Boyd, 1966) and corresponds with the results of Green and Ringwood (1967) using similar bulk compositions.

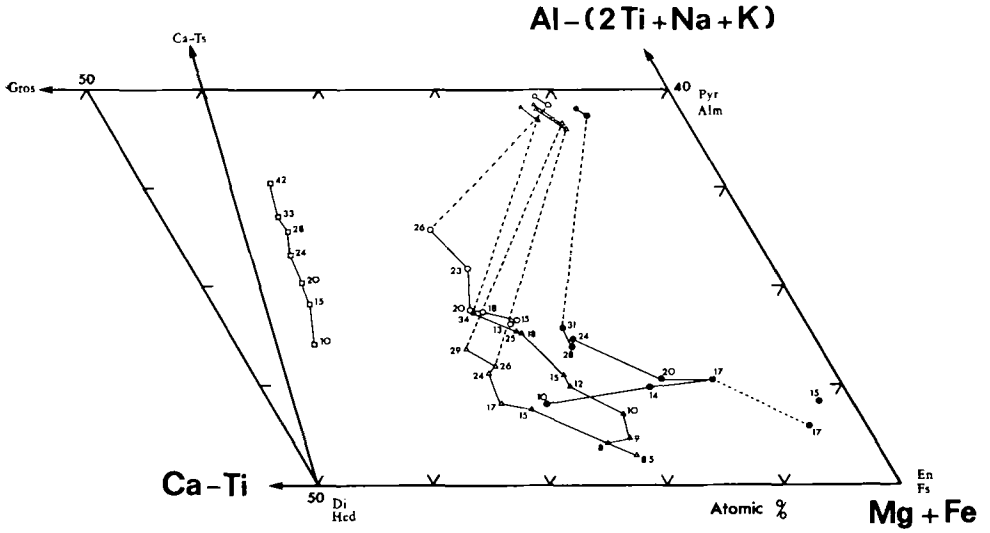

FIG. 8. A–C–FM diagram for the near-liquidus pyroxenes of Table II. Symbols as in fig. 1. Allowance is made for Ca and Al in $CaTiAl_2O_6$ and for Al in $NaAlSi_2O_6$ component in the pyroxenes. Garnets are plotted using the same conventions as the pyroxenes and *also* (small symbols) with *no* adjustments to Ca and Al values. Broken lines join coexisting pyroxenes and garnets. The crystallization pressure (in kb) is marked beside each pyroxene.

Solid solution between pyroxenes and garnets. The complex interplay between Ca, Al, and Fe–Mg along the near-liquidus pyroxene trends in Table II is most clearly shown in fig. 8. This is an A–C–FM diagram in atomic percent (to conform with previous figs.), with allowance made for Ca and Al used in $CaTiAl_2O_6$ and $NaAlSi_2O_6$ substitutions. This diagram has been used to depict both natural and synthetic high-pressure pyroxene chemical variation and pyroxene–garnet relations by many previous authors, such as Yoder and Tilley (1962), O'Hara and Yoder (1967), Kushiro and Aoki (1968), Kuno (1969), Lovering and White (1969), Beeson and Jackson (1970), and Boyd (1970). A curious feature of this diagram is that almost every author that has used it has employed a different convention for calculating the positions of the plotted points. Visual comparisons between published versions should therefore be made with great caution.

The pyroxenes on fig. 8 show extensive solid solution towards garnet at high pressures. The amount of solid solution of the Ca-rich pyroxenes towards Ca-poor pyroxene and the Al content at which they coexist with garnet varies greatly from set to set. It was pointed out previously that there seems to be no simple relationship between these features and the bulk compositions of the rocks. The reduced solubility of Ca-poor pyroxene in Ca-rich pyroxenes with increasing Al substitution at high pressure is consistent with the interpretations of pyroxene relations made by O'Hara and Yoder (1967) and Boyd (1970), but with a slightly different emphasis from these authors. They were mainly concerned with the effect of varying bulk composition at constant values of P, whereas fig. 8 evaluates the effect of changing P (and T) on the pyroxenes precipitating from five constant bulk compositions. It is noticeable on fig. 8 that in some of the sets, particularly 66018, considerable pressures are attained before the influence of Al substitution predominates over the opposing effect of increasing solid solution towards Ca-poor pyroxene with rising temperature along the anhydrous liquidi. The four sets of pyroxenes on fig. 8 with broadly similar Ca/(Mg+Fe) ratios show a crude correlation between their Mg/Fe ratios and the pressure at which the inflection away from the FM apex of fig. 8 occurs.

Ti *in high-pressure pyroxenes.* One of the surprising results of this study is the evidence on fig. 4 that Ti increases with rising pressure at constant temperature in these complex pyroxenes crystallized from natural rock compositions. Yagi and Onuma (1967) studied the join $CaMgSi_2O_6$–$CaTiAl_2O_6$ experimentally and showed that, although extensive solid solution of $CaTiAl_2O_6$ in diopside occurred at one atmosphere, this was reduced almost to zero at 1000 °C and pressures between 10 and 25 kb. It has become widely accepted by subsequent authors that pressure reduces the substitution of Ti in Ca-rich pyroxene. The new data contradict this hypothesis, but show that pyroxenes crystallized from mafic magmas at depth are likely to have comparatively low Ti contents due to their high *temperatures* of formation. Presumably the explanation of why these results differ from those of Yagi and Onuma (1967) lies in the greater number of components in the pyroxenes formed from rock melts. Possibly Na is the vital extra component, with a reaction such as

$$CaTiAl_2O_6 + NaFe^{3+}Si_2O_6 \rightleftharpoons NaTiAlSiO_6 + CaFe^{3+}AlSiO_6 \qquad (1)$$

moving to the right with increasing pressure. Pyroxenes supposed to have formed at high pressures and containing relatively large amounts of Ti have been reported by Aoki and Kushiro (1968) and Binns, Duggan, and Wilkinson (1970). M. F. J. Flower, Ruhruniversität Bochum (personal communication) has recently found pyroxene of the composition $NaTiAlSiO_6$ to be stable at 30 kb.

Fe^{3+} *in the augite leucitite pyroxenes.* The pyroxene analyses in Table II have been calculated into 'molecules' according to the conventions proposed by Kushiro (1962). The members of each near-liquidus set that were formed at high pressures contain considerable amounts of the jadeite ($NaAlSi_2O_6$) and Ca-Tschermak's ($CaAl_2SiO_6$) molecules. All the iron in these pyroxenes has been assumed to be Fe^{2+} when making the calculations. This procedure maximizes their jadeite contents compared with those of most published analyses of naturally occurring pyroxenes, because the latter

contain varying amounts of Fe^{3+}. Kushiro (1962), White (1964), and all subsequent authors who considered the problem have proposed that allocation of Na to Fe^{3+} to form acmite ($NaFeSi_2O_6$) should preceed allocation of Al to the remaining Na, if any, to form jadeite molecule in the recalculation of a pyroxene analysis. This procedure leads to major difficulties with the augite leucitite (EU 13) pyroxene set in Table II.

The stoichiometry of the EU 13 pyroxenes (Table II) suggests that they contain considerable amounts of Fe^{3+}, in contrast with the other pyroxene sets, which closely fit a 4 cation, 6 oxygen formula with all Fe taken as Fe^{2+}. Calculation of the Fe^{3+} in a mineral by consideration of the stoichiometry of a microprobe analysis is subject to substantial error (Finger, 1972). However, the surprising feature of the near-liquidus EU 13 pyroxenes is that their stoichiometry, with all Fe taken as Fe^{2+}, shows progressive changes (fig. 9) with rising pressure and temperature. This is most simply interpreted to mean that Fe^{3+} in these pyroxenes falls with increasing pressure along the near-liquidus trend up to about 28 kb and then remains constant with further rising pressure. Fig. 9 also shows the stoichiometry of these pyroxenes plotted as a function of their Na contents. This reveals that such correlation as there is between Na and Fe^{3+} is *negative* and that, in any case, the correlation is poor because Na continues to rise steadily above 28 kb when the cation sum becomes constant. The parallelism between the two curves on fig. 9 results from the excellent correlation between Na and pressure in this set (Table II).

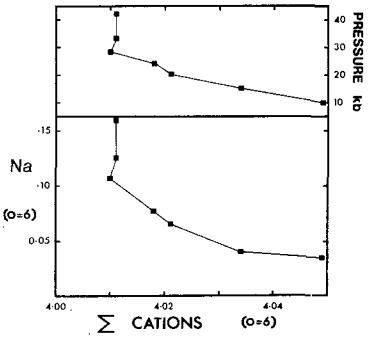

FIG. 9. Cation sums (all Fe as FeO) on a 6 oxygen basis of EU13 near-liquidus pyroxenes plotted as functions of their Na contents and pressures of formation.

The relationships shown in Fig. 9 lead to this question: why should Na and Fe^{3+} be combined as acmite molecule in the recalculation of these pyroxenes when they show no semblance of a positive correlation? Surely in this particular set of analyses it is more logical to allocate all the Na to jadeite molecule? A possible equation to show this manipulation would be

$$NaFe^{3+}Si_2O_6 + CaAlFe^{3+}SiO_6 \rightleftharpoons NaAlSi_2O_6 + CaFe^{3+}Fe^{3+}SiO_6, \qquad (2)$$

with the implication that the ferridiopside ($CaFe_2SiO_6$) molecule breaks down at high pressure. The role of $CaAlFe^{3+}SiO_6$ molecule is inconsistent between equation 1, where it is a product and equation 2, where it is a reagent. The allocation of Fe^{3+} and Al to the tetrahedral and octahedral lattice sites in $CaAlFeSiO_6$ is also implied to be different between equations 1 and 2. This corresponds with current knowledge of the ease with which Fe^{3+}, in addition to Al, can substitute for Si in the tetrahedral sites of pyroxenes (Virgo, 1972), and our lack of knowledge about the extent to which this happens in various circumstances. The traditional procedure of allocating Al to make up Si deficiency in a pyroxene formula is, like priority for acmite formation, a matter of *convention*. However, this seems to be unavoidable without much more information

on the behaviour of Fe^{3+} in clinopyroxenes. It is also fortunately unimportant in the present discussion, which simply aims to emphasize that the recalculation of pyroxene analyses into 'molecules' is an arbitrary procedure, particularly in the absence of crystallographic site-occupancy data. This has evolved rules and conventions that may give authors scope for discussions (e.g. White, 1964) but must of course *never* be allowed to obscure rather than assist the discovery of significant chemical variation in sets of pyroxenes, a point stressed by Kuno (1969, p. 219).

A final matter to note is the implication in the foregoing section that pyroxenes containing significant amounts of Fe^{3+} crystallize from a strongly alkalic and silica-undersaturated melt (EU 13) at levels of f_{O_2} where the pyroxenes precipitating from less alkalic and undersaturated basaltic melts appear to be essentially Fe^{3+}-free. It has long been known that alkali basalts and strongly alkalic mafic rocks are generally progressively more oxidized, in terms of Fe^{2+}/Fe^{3+} ratio, than tholeiitic basalts. Most authors have attributed this to higher f_{O_2}, produced by an assumed greater volatile content in the alkalic magmas, or have used the data as evidence for one. However, it has also been suggested (e.g. Lindsley, Carmichael, and Nicholls, 1968) that perhaps f_{O_2} levels in the various magma types do *not* vary greatly but nevertheless produce differing degrees of oxidation, due to changes in the activity coefficients of FeO and Fe_2O_3 in the magmas of differing composition. The pyroxene data reported here are a scrap of direct experimental evidence that the second hypothesis is correct.

Comparison of synthetic pyroxenes with naturally occurring supposedly high-pressure pyroxenes. During the last few years many descriptions have been published of pyroxenes forming megacrysts or coarsely crystalline inclusions in lavas or pyroclastic rocks. These are frequently postulated to have crystallized at high pressures; the most often-quoted evidence for this being that they contain substantial amounts of octahedrally coordinated Al or that they are associated with phases such as garnet or aluminous spinel, which could only precipitate at high pressures from melts with compositions similar to the rocks in which they are found. Several discussions, such as those of White (1964), O'Hara (1967), Aoki and Kushiro (1968), and Lovering and White (1969), have been concerned with disentangling the effects of pressure and temperature upon the compositions of such pyroxenes and with establishing diagrammatic means for determining the physical conditions in which pyroxenes of supposed high-pressure origins crystallized, either in terms of the generalized *P–T* concepts of metamorphic facies (White, 1964; Aoki and Kushiro, 1968; Lovering and White, 1969; O'Hara, 1969) or as a numerical *P–T* grid (O'Hara, 1967). It would be impractical to make a detailed comparison here between the new data and all these diagrams. Instead one of the most commonly used diagrams is discussed, in order to show in a general way how the analyses in Table II correlate with current views on this subject.

The jadeite and Ca-Tschermak's molecules (Table II) of all the new Ca-rich pyroxene analyses are plotted on fig. 10. The five near-liquidus trends are shown by solid lines, whilst dashed lines mark the side-trends of pyroxenes formed with falling temperature at constant pressure (see figs. 4–6). Although, as shown above, the EU 13 pyroxenes appear to contain some Fe^{3+}, all of their Na has been allocated to Al to

form jadeite on fig. 10, following the procedure suggested in the previous section. In this form the diagram shows several interesting features. Firstly, both jadeite and Ca-Tschermak's molecule increase steadily with rising pressure and temperature along the five near-liquidus trends, except during the solid solution excursions towards Ca-poor pyroxene (see fig. 8) in the 66018 and 59-P-13 sets. Secondly, if these near-liquidus pyroxene trends are extrapolated at their low-pressure ends, it seems probable that at one atmosphere the five bulk compositions studied would precipitate pyroxenes containing little or no jadeite but widely varying amounts of Ca-Tschermak's molecule. Thirdly, the near-liquidus trends radiate to cover a wide field of the diagram, so that a given pressure or temperature in the various pyroxene sets corresponds with very different Jd and Ca-Ts contents.

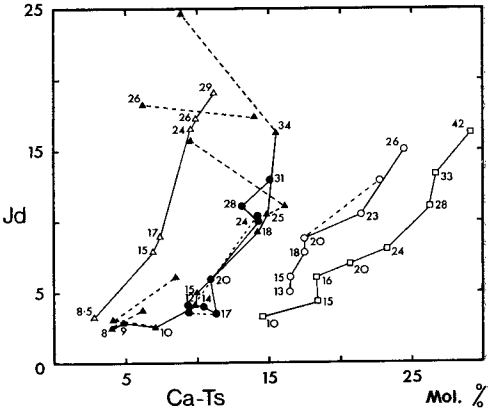

FIG. 10. Jadeite versus Ca-Tschermak's component for the near-liquidus pyroxenes of Table II and associated pyroxenes formed at lower temperatures within the melting ranges of 66018, SK971, and 59-P-13. Solid lines denote the near-liquidus trends. Broken lines indicate trends of falling temperature at constant pressure. Symbols are as in fig. 1. The crystallization pressure (in kb) is marked beside each near-liquidus pyroxene.

The side trends on fig. 10 of pyroxenes formed with decreasing temperatures at constant pressures are of two types: If the pyroxenes co-precipitate with garnet, their jadeite contents rise and Ca-Tschermak's molecule contents fall with decreasing temperature. O'Hara (1969) noted the same trend in a subsolidus experimental study of natural magnesian-garnet–clinopyroxene pairs (see fig. 11B below). If the pyroxenes crystallize without coexisting garnet, their Jd and Ca–Ts contents both rise with falling temperature, so that the side trend is parallel to the main near-liquidus trend.

The jadeite and Ca-Tschermak's molecules of a selection of natural Ca-rich pyroxenes occurring as megacrysts or inclusions in volcanic rocks are plotted on fig. 11A. The recalculation of these analyses has *not* been made according to the scheme of Kushiro (1962). Instead, for reasons explained above, Na has been allocated first with Al to jadeite molecule and the formation of acmite restricted to pyroxenes where Na exceeds Al^{vi}. The natural pyroxenes plot in the same region of fig. 11A when treated this way as do the near-liquidus synthetic pyroxene sets on fig. 10.

It is immediately tempting to look for similarities of pattern between the data sets of figs. 10 and 11A. However, such comparisons should be made with great care. A suite of megacrysts or inclusions may have precipitated from a single batch of magma but, if they had separated in any abundance, the residual liquid would of course have changed composition so that the pyroxenes were *not* formed from a melt of a single composition. Alternatively, pyroxenes in a suite might have crystallized from a number

of distinct magma batches, which might be of similar general character but unrelated in detail. After their formation the pyroxenes may have partially re-equilibrated to lower pressure or temperature conditions (or both), but even the various pyroxenes in a single suite may not all have done this to the same extent.

In contrast, the near-liquidus synthetic pyroxene sets (fig. 10) have each crystallized

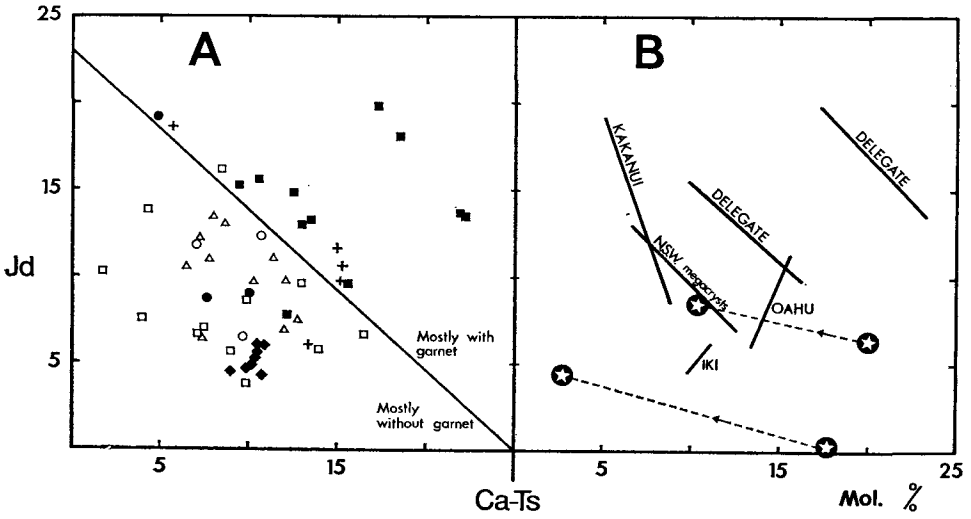

FIG. 11. Jadeite versus Ca-Tschermak's component for naturally occurring Ca-rich pyroxenes forming megacrysts or coarse grained inclusions in lavas or pyroclastic rocks. All those plotted in section A have been postulated to have formed at high pressures in their previously published descriptions. Jadeite contents are calculated on an Fe_2O_3-free basis (see text for discussion). Symbols on A indicate the sources of the data thus: filled squares = Delegate, Australia (Lovering and White, 1969); open squares = Eifel, Germany (Aoki and Kushiro, 1968); filled circles = Kakanui, New Zealand (Dickey, 1968); open circles = Grand Canyon, U.S.A. (Best, 1970); filled diamonds = Iki, Japan (Aoki, 1968); open triangles = NE New South Wales (Binns *et al.*, 1970); crosses = Salt Lake Crater, Oahu, Hawaii (Beeson and Jackson, 1970). Solid lines in section B indicate variation trends within the sets of points in A, for comparison with the experimental data of fig. 10. In addition, broken lines join two pairs of magnesian Ca-rich pyroxenes coexisting with garnet at constant pressure and falling temperature (direction of arrow), reported by O'Hara (1969).

from a single specific bulk composition. This is not necessarily one that ever existed in the earth within at least part of the pressure range used in the experiments. Consideration of the *P–T* diagrams for each lava (Thompson, 1972, 1973, 1974) suggests that the approximate pre-eruption equilibration pressures of the magmas were: 66018, 17 kb; SK971, 10 kb; 59-P-13, 8 kb; OB32, 8 kb; EU13, 14 kb.

Despite these reservations, there are several interesting points of comparison between figs. 10 and 11A. On fig. 11A the diagonal line from 23 % Jd to 25 % Ca-Ts divides with 90 % efficiency pyroxenes that coexist with garnet (above to right) from those that do not (below to left). No similar straight line can be drawn on fig. 10 but, apart from the leucitite (EU 13) set, the pyroxenes with and without associated garnet in the synthetic sets occupy similar parts of the diagram to those of their natural analogues.

The more restricted field of the natural pyroxenes on fig. 11A compared to that of the synthetics on fig. 10 may indicate that the former have precipitated from a more limited range of compositions in nature, or within a narrower *P–T* interval than the compositions and physical conditions used in the experimental study. Even if this is true, it does not lessen the importance of the point that is so clearly apparent in fig. 10 and has been stressed throughout the discussion of previous diagrams: namely that by far the most important factor controlling the composition of a pyroxene precipitated within a given broad range of pressures and temperatures is the composition of the melt from which it crystallized. This means that, unless a suite of natural megacrysts or xenolith pyroxenes have all separated from a single batch of magma and in sufficiently small quantities not to affect its composition significantly, it is unlikely that consideration of their chemical variation will be able to indicate anything about the relative *P–T* conditions of their formation.

Although the parameters of figs. 10 and 11 are the same in name as those used by White (1964), the 'acmite last' convention used here in calculating the jadeite component makes these figures closely approach the Al^{vi}–Al^{iv} diagram used by Aoki and Kushiro (1968). At first sight it is curious that the lines used by both White (1964) and Aoki and Kushiro (1968) to separate what they regarded as groups of pyroxenes formed under distinctive physical conditions should radiate from the origins of their diagrams, thus falling *sub-parallel* to the trends of the near-liquidus pyroxene sets on fig. 10. However, this simply reflects the rather distinctive grouping on this type of plot of the natural pyroxenes discussed by these workers and others, such as Lovering and White (1969) and Kuno (1969). All these authors tend to compare and contrast 'granulite facies' pyroxenes from high-grade metamorphic rocks and megacrysts and inclusions in alkalic lavas with 'eclogite facies' pyroxenes from blueschist metamorphic areas and inclusions in kimberlites. Clearly both facies occupy very wide pressure ranges, with P_{H_2O} at low levels (Fry and Fyfe, 1969; Brown and Fyfe, 1972). It is the relative *temperature* of formation at a given pressure (on a sliding scale of increasing overall *T* with rising *P*) that seems to distinguish granulite from eclogite facies. On a Jd–Ca-Ts diagram the pyroxenes of generally accepted eclogites, such as kimberlite inclusions, fall at the low-temperature ends of equilibration trends of pyroxene *co-existing with garnet* with falling temperature at a given pressure. The pyroxenes of more controversial garnet pyroxenites, such as the Oahu inclusions (White, 1964; Green, 1966; O'Hara, 1969; Kuno, 1969; Beeson and Jackson, 1970), fall along the higher-temperature parts of these trends. Reference to fig. 10 and the data (fig. 11B) of O'Hara (1969) will show that these 'with garnet' equilibration trends are approximately at right angles to the near-liquidus pyroxene trends on fig. 10.

Although the new data can be used to illuminate previous studies of a wide variety of high-pressure pyroxenes, as shown above, they should clearly find their main application in interpreting and predicting the chemical variation of pyroxenes thought to have formed in equilibrium with a magma at depth and quenched without prolonged sub-solidus re-equilibration. In fig. 11B an attempt is made to begin this process by locating variation trends amongst the natural pyroxene suites of fig. 11A. Obviously, as the reader can see, several of the trends indicated on fig. 11B are drawn from very

scattered groups of points on fig. 11A. However, two sets, the Iki megacrysts and the (Jd+Ca-Ts)-rich Delegate pyroxenes, show excellent linear variation. At the other extreme, the dispersal of the Dreiser Weiher data on fig. 11A supports Aoki and Kushiro's (1968) view that these pyroxenes crystallized from a variety of associated mafic magmas, rather than a single liquid. Thus, the effect of bulk composition has swamped those of P and T upon the chemistry of the pyroxenes.

The outstanding feature of the trends on fig. 11B is that their directions are not random but clearly fall into two groups, which are approximately at right angles to each other and sub-parallel to the two trend directions that fit all the synthetic data on fig. 10. The Delegate and Kakanui pyroxenes coexist with garnet and the direction of their variation trends on fig. 11B, parallel to the 'with garnet' falling T at constant P trends on fig. 10, is reasonable. However, the N.S.W. megacryst pyroxenes are from garnet-free assemblages. Possibly they were precipitated from a set of similar but slightly varying magmas at roughly constant P and T. This concept fits well with their occurrence in lavas having an appreciable variety of compositions (Binns *et al.*, 1970). Alternatively, it may be significant that these pyroxenes coexist with aluminous spinel (Binns *et al.*, 1970, table 8). Perhaps the 'with spinel' trend is in the same direction as the 'with garnet' trends on fig. 10.

Acknowledgements. The experimental studies and microprobe analyses were made at the Geophysical Laboratory, Carnegie Institution of Washington. I. Kushiro was a constant source of stimulating discussion on pyroxene chemistry and phase relations. It is also a pleasure to thank him, together with J. Akella, P. M. Bell, and B. J. Hensen, for assistance and advice on all aspects of the experiments. L. W. Finger and C. G. Hadidiacos provided invaluable tuition in the use of automated microprobe.

REFERENCES

Aoki (K.), 1968. *Amer. Min.* **53**, 241.
—— and Kushiro (I.), 1968. *Contr. Min. Petr.* **18**, 326.
Banno (S.) and Matsui (Y.), 1965. *Proc. Jap. Acad.* **41**, 716.
Beeson (M. H.) and Jackson (E. D.), 1970. *Min. Soc. Amer. Spec. Paper*, **3**, 95.
Bence (A. E.) and Albee (A. L.), 1968. *Journ. Geology*, **76**, 382.
Best (M. G.), 1970. *Contr. Min. Petr.* **27**, 25.
Binns (R. A.), Duggan (M. B.), and Wilkinson (J. F. G.), 1970. *Amer. Journ. Sci.* **269**, 132.
Boyd (F. R.), 1968. *Carnegie Instn. Washington, Yearbook*, **66**, 327.
—— 1970. *Min. Soc. Amer. Spec. Paper*, **3**, 63.
—— and Schairer (J. F.), 1964. *Journ. Petrology*, **5**, 275.
Brown (G. C.) and Fyfe (W. S.), 1972. *Proc. 24th Int. Geol. Congress Sect.* **2**, 27.
Bultitude (R. J.) and Green (D. H.), 1971. *Journ. Petrology*, **12**, 121.
Davis (B. T. C.) and Boyd (F. R.), 1966. *Journ. Geophys. Res.* **71**, 3567.
Dickey (J. S.), 1968. *Amer. Min.* **53**, 1304.
Erlank (A. J.), and Kushiro (I.), 1970. *Carnegie Instn. Washington, Yearbook*, **68**, 233.
Finger (L. W.), 1972. Ibid. **71**, 600.
—— and Hadidiacos (C. G.), 1971. Ibid. **70**, 269.
Fry (N.) and Fyfe (W. S.), 1969. *Contr. Min. Petr.* **24**, 1.
Green (D. H.), 1966. *Earth Planet. Sci. Lett.* **1**, 414.
—— and Hibberson (W.), 1970. *Phys. Earth Planet. Interiors*, **3**, 247.
—— and Ringwood (A. E.), 1967. *Contr. Min. Petr.* **15**, 103.
Green (T. H.) and Ringwood (A. E.), 1968. Ibid. **18**, 105.
Kuno (H.), 1969. *Geol. Soc. Amer. Mem.* **115**, 189.
Kushiro (I.), 1962. *Japan Journ. Geol. and Geog.* **33**, 213.

KUSHIRO (I.) and AOKI (K.), 1968. *Amer. Min.* **53**, 1347.
LINDSLEY (D. H.), CARMICHAEL (I. S. E.), and NICHOLLS (J.), 1968. *Journ. Geophys. Res.* **73**, 3351.
LOVERING (J. F.) and WHITE (A. J. R.), 1969. *Contr. Min. Petr.* **21**, 9.
O'HARA (M. J.), 1967. In *Ultramafic and Related Rocks* (ed. P. J. WYLLIE) New York (John Wiley), 393.
—— 1969. *Geol. Mag.* **106**, 322.
—— and YODER (H. S.), 1967. *Scott. Journ. Geol.* **3**, 67.
ROEDER (P. L.) and EMSLIE (R. F.), 1970. *Contr. Min. Petr.* **29**, 275.
SMITH (D.) and LINDSLEY (D. H.), 1971. *Amer. Min.* **56**, 225.
THOMPSON (R. N.), 1972. *Carnegie Instn. Washington, Yearbook*, **71**, 406.
—— 1973. *Journ. Geol. Soc. London*, **129**, 649.
—— 1974. Ibid., **130**, 181.
—— ESSON (J.), and DUNHAM (A. C.), 1972. *Journ. Petrology*, **13**, 219.
—— and FLOWER (M. F. J.), 1971. *Earth Planet. Sci. Lett.* **12**, 97.
—— and KUSHIRO (I.), 1972. *Carnegie Instn. Washington, Yearbook*, **71**, 615.
TILLEY (C. E.) and THOMPSON (R. N.), 1970. *Earth Planet. Sci. Lett.* **8**, 79.
—— —— 1972. *Geol. Journ.* **8**, 65.
VIRGO (D.), 1972. *Carnegie Instn. Washington, Yearbook*, **71**, 534.
WHITE (A. J. R.), 1964. *Amer. Min.* **49**, 883.
YAGI (K.) and ONUMA (K.), 1967. *Journ. Fac. Sci. Hokkaido Univ., Ser.* 4, **13**, 463.
YODER (H. S.) and TILLEY (C. E.), 1962. *Journ. Petrology*, **3**, 342.

[*Manuscript received 11 December 1973.*]

Note added in proof: A full account of the high-pressure melting behaviour of Skye basalts 66018 and SK971 is now published (*Contr. Min. Petr.* **45**, 317). This contains analyses of the garnets and sub-liquidus pyroxenes crystallized during experiments on these lavas and described above.